Electronic Supplementary Material (ESI) for Journal of Materials Chemistry A.

Supporting Information

Cs^+ incorporation into $CH_3NH_3PbI_3$ perovskite: Broad miscibility gap and stability enhancement

Ralf G. Niemann[a], Laxman Gouda[b], Jiangang Hu[b], Shay Tirosh[b], Ronen Gottesman[b], P.J. Cameron[a] and Arie Zaban[b]

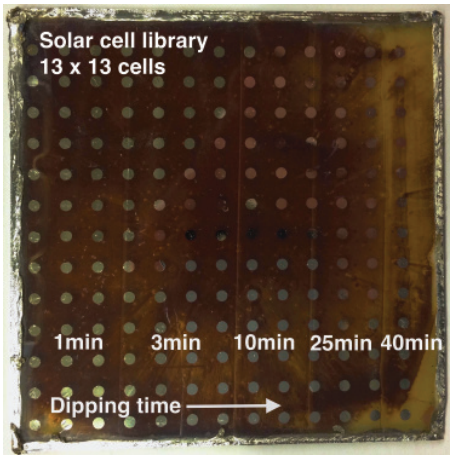

Figure E1: An example of a solar cell library (13 x 13 cells) with a gradient perovskite layer after dipping into a CsI in IPA solution.

Table E1: Fittings of the (110) reflection during in-situ cation exchange.

Time	2Θ [°]
0min	14.13
3min	14.16
8min	14.17
18min	14.17
28min	14.18
38min	no peak

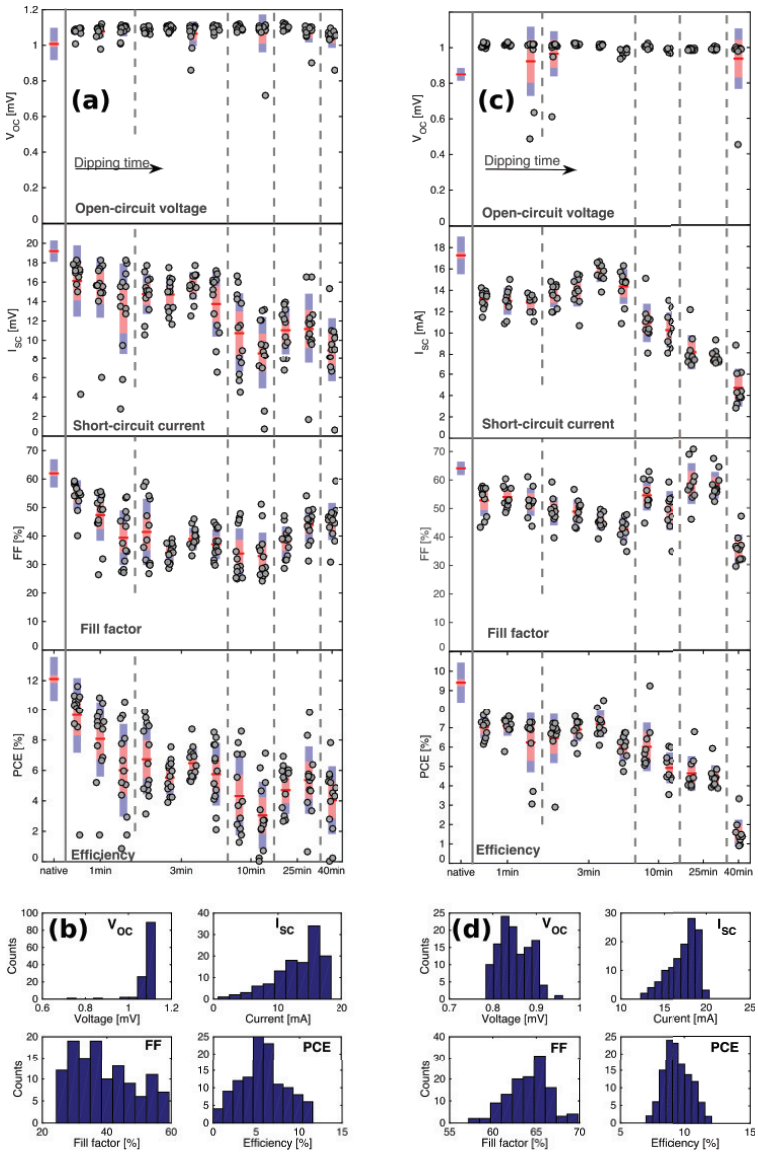

Figure E2: A summary is given of the photovoltaic parameters over dipping time for two different batches, namely open-circuit voltage V_{OC}, short-circuit current I_{SC}, fill factor FF and power conversion efficiency PCE, respectively. (a+c) shows the full parameter distribution with each cell indicated as a dot, while (b+d) shows the distribution of those parameters for the native sample in form of a histogram. The qualitative trend is the same in that the V_{OC} increases upon Cs-incorporation and I_{SC} (and therefore PCE continuously drop for increasing dipping times. The blank sample shown in (d) shows a broader distribution of most PV parameters, but the qualitative response of the parameters for the Cs^+ dipping remains the same.

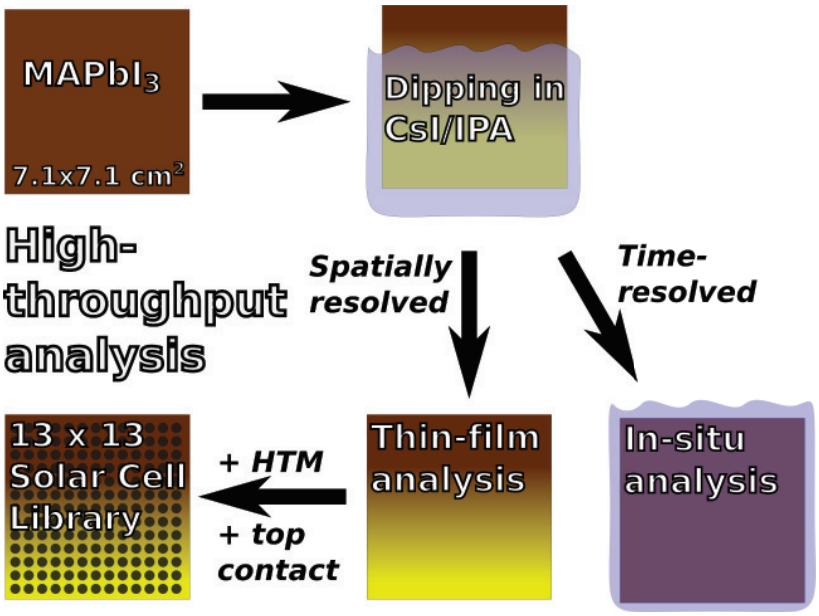

Figure E3: Synthesis and analysis of Cs+ incorporated MAPbI3 solar cells. A gradual dipping conversion was done on 7 7 cm2 substrates. The optical, electronic and structural properties of the material were tested in a high-throughput fashion. In-situ measurements were taken to clarify the conversion mechanism and show the improved stability of CsxMA1-xPbI3. Analysis of the thin-films and solar cells gave information about the material and its photovoltaic performance.

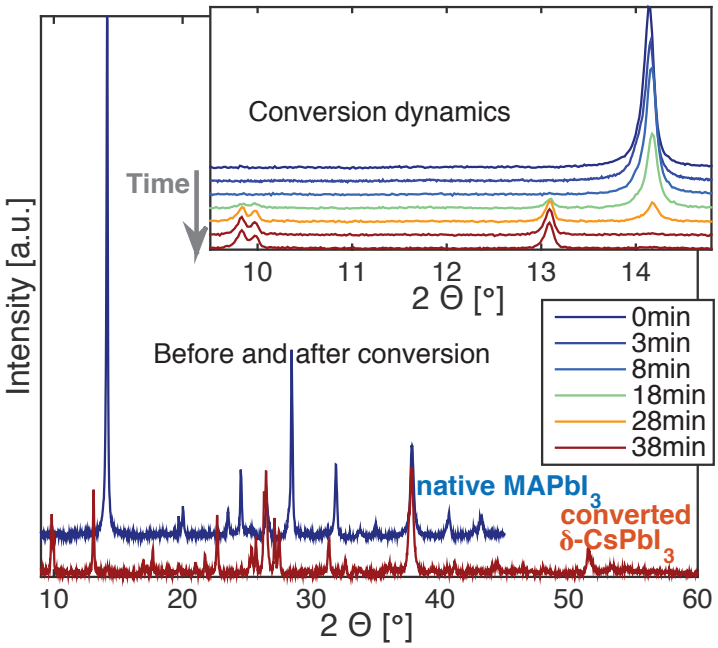

Figure E4: full XRD spectra of the in-situ cation exchange shows the complete conversion within the 38min of the experiment. The inset shows zoomed-in diffractograms at different stages of the conversion process.

Table E2: Peak position of (110) reflection found in diffractions done for different $Cs_xMA_{1-x}PbI_3$ compositions made with a one-step deposition. Peak position obtained using fittings of the (110) reflection peak to a calculated pseudoVogit intensity profile done in CrystalMaker. The full diffractograms can be found in fig. 2 in the main document.

Composition	2Θ [°]
x=0	14.17
x=5	14.19
x=10	14.21
x=15	14.23
x=20	14.20
x=25	14.20
x=30	14.21
x=40	14.19
x=50	14.23
x=75	14.34
x=100	-

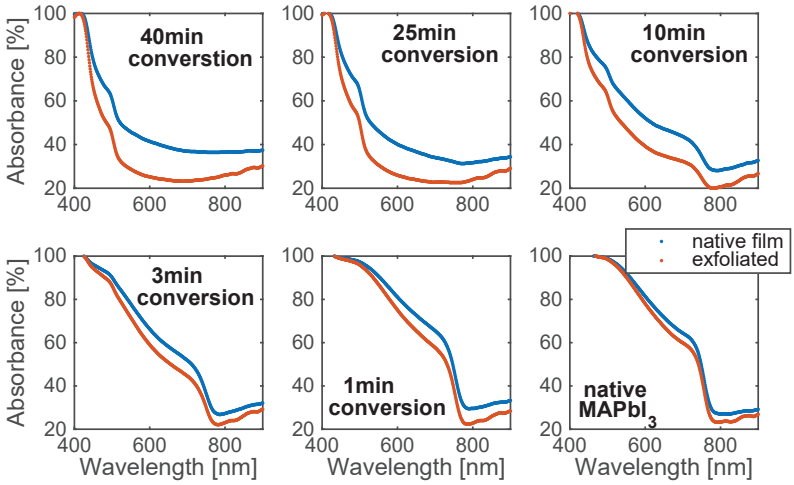

(a)

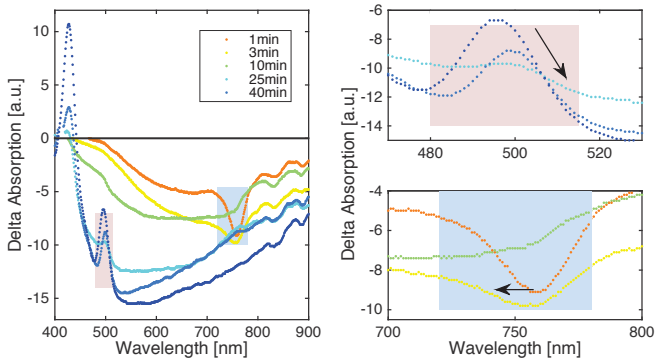

(b)

Figure E5: (a) UV-Vis spectra of different conversion stages of the native thin-films (native $MAPbI_3$ and different conversion times in CsI solution). (b) The subtracted spectra before baseline removal. The baseline corrected spectra are shown in fig. 5 in the main document.

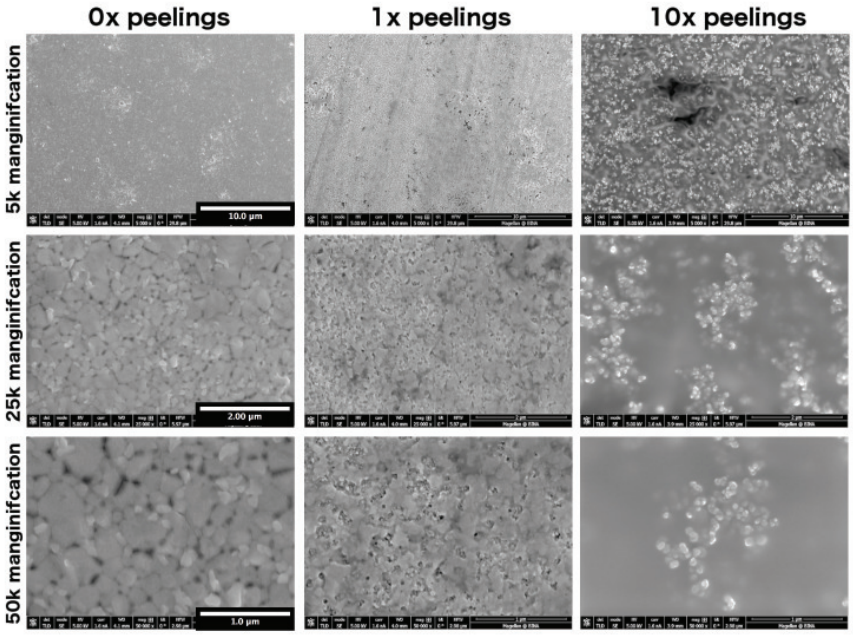

Figure E6: SEM images taken at different stages of the peeling process on $MAPbI_3$ ting(before, after one peeling and ten peelings). Results show the incremental removal of the capping layer.

Table E3: Structural parameters of the plain perovskites $MAPbI_3$ and $CsPbI_3$ as well as the mixed cation $Cs_xMA_{1-x}PbI_3$ in their cubic phase. Namely the cation radii r_{cation} [1] and unit cell volume $V_{UC,cubic}$ [2] were taken from literature. The values of the (110) reflection in XRD (2 Θ) and corresponding d-spacing as measured in this study.

Perovskite cation		MA	Cs_xMA_{1-x}	Cs	Rel. diff.
Literature	r_{cation} [1]	2.17 Å		1.81 Å	-16.6 %
	$V_{UC,cubic}$ [2]	251.6 $Å^3$		248.8 $Å^3$	-1.12 %
Measured	2 Θ (110)	14.14 °	14.18 °		0.30 %
	d-spacing	6.26 Å	6.24 Å		-0.30 %

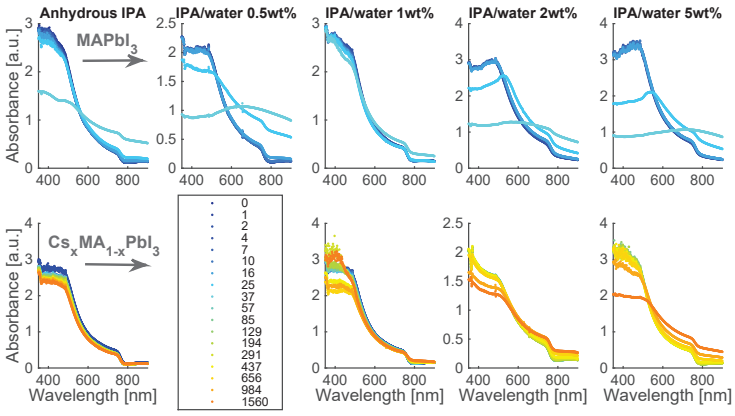

Figure E7: UV-Vis absorption spectra of thin-films (native $MAPbI_3$ above and $Cs_xMA1-xPbI_3$ below) dipped into a solution of IPA with different concentrations of water. The absorption in the blue regime dropped significantly as the thin-films decomposed into PbI_2, alongside an increase of the red regime, caused by scattering. A drop of the signal at 450 nm of 80 % was defined as the time of degradation. $Cs_xMA1-xPbI_3$ in solutions of water/IPA < 0.02 were stable over the full duration of the measurement (10h) and remained without visible color change for more than a week.

Error analysis

The propagation of error calculations were calculated individually for the three different approaches that were taken in this study (Tauc plot, EDAX and XRD).

Tauc plot error: The shift of the bandgap was determined via Tauc plot. Therefore, we fitted a first order polynomial to the linear region of the Tauc plot of the $Cs_xMA_{1-x}PbI_3$ after cation conversion (Tauc 1 with bandgap T_1) and for the blank $MAPbI_3$ (Tauc 2 with T_2). The linear fit parameters for Tauc 1 plot curve with standard deviation are $a_1 = 0.1775 \pm 0.0009 \cdot 10^{-23}$ and $c_1 = -0.2851 \pm 0.0014 \cdot 10^{-23}$. The intersection with the x axis and corresponding error function are:

$$T_1 = \frac{c_1}{a_1} \qquad \Rightarrow \Delta T_1 = \pm\sqrt{\left(\Delta c_1 \frac{1}{a_1}\right)^2 + \left(\Delta a_1 \frac{c_1}{a_1^2}\right)^2}$$

$$\Rightarrow T_1 = 1.618 \pm 0.012 \text{ eV}$$

For the blank $MAPbI_3$ sample we performed and analogous calculation with the fit parameters of the linear region of Tauc 2 of $a_2 = 0.1842 \pm 0.00015 \cdot 10^{-23}$ and $c_2 = -0.2946 \pm 0.0002 \cdot 10^{-23}$. The intersection with the x axis and corresponding error function are:

$$T_2 = \frac{c_2}{a_2} \qquad \Rightarrow \Delta T_2 = \pm\sqrt{\left(\Delta c_2 \frac{1}{a_2}\right)^2 + \left(\Delta a_2 \frac{c_2}{a_2^2}\right)^2}$$

$$\Rightarrow T_2 = 1.598 \pm 0.0018 \text{ eV}$$

The value for the bandgap of pure $CsPbI_3$ is taken from literature[2] $T_3 = 1.73$ eV. Combining these values we can calculate the composition from our UV-Vis measurements and the corresponding error function:

$$x_{Tauc} = \frac{T_2 - T_1}{T_3 - T_1} \qquad \Rightarrow \Delta x_{Tauc} = \pm\sqrt{\left[\Delta T_2 \frac{T_1 - T_2}{(T_3 - T_2)^2}\right]^2 + \left(\Delta T_1 \frac{1}{T_3 - T_2}\right)^2}$$

$$\Rightarrow \Delta x_{Tauc} = \pm 0.081$$

EDAX error: The constant regime (*step I*) of the absorbance at 450 nm is evaluated by forming the mean average $c_1 = 2.850 \pm 0.047$, while the slope that occurs during the *step II* conversion is fitted with a first order polynomial ($y = a \cdot x + b$) with $a_2 = 0.407 \pm 0.021$ and $b_2 = -1.47 \pm 0.18$. The slope of the EDAX Cs signal was also fitted with a first order polynomial with $a_3 = -0.0466 \pm 0.0018$ and $b_3 = 0.602 \pm 0.016$. The formula to determine composition x_{EDAX} derives from simple geometric consideration to:

$$x_{EDAX} = a_3 \frac{c_1 - b_2}{a_2} + b_3$$

$$\Rightarrow \Delta x_{EDAX} =$$

$$\pm\sqrt{\left[\Delta a_3\frac{c_1-b_2}{a_2}\right]^2+\left[\Delta c_1\frac{a_3}{a_2}\right]^2+\left[\Delta b_2\frac{a_3}{a_2}\right]^2+\left[\Delta a_2\frac{a_3}{a_2^2}(c_1-b_2)\right]^2+\Delta b_3^2}$$

$$\Rightarrow \Delta x_{EDAX} = \pm 0.042$$

XRD error: The miscibility gap estimation from XRD was done by measureing the (110) reflection peak of different stoichiometric $Cs_xMA_{1-x}PbI_3$ thin-films. The shifting reflection peaks were fitted with a first order polynomial with a slope $a = 0.4012 \pm 0.048$. This slope was compared to the obtained shift during the cation conversion, with (110) reflection before conversion of $\Theta_1 = 14.137 \pm 0.0037\ ^\circ$ and after 28 min conversion $\Theta_2 = 14.184 \pm 0.0098\ ^\circ$. The function to calculate the composition and the according error function are:

$$x_{XRD} = \frac{\Theta_2 - \Theta_1}{a}$$

$$\Rightarrow \Delta x_{XRD} = \pm\sqrt{\left[\Delta a\frac{\Theta_2-\Theta_2}{a^2}\right]^2+\left(\Delta\Theta_1\frac{1}{a}\right)^2+\left(\Delta\Theta_2\frac{1}{a}\right)^2}$$

$$\Rightarrow \Delta x_{XRD} = \pm 0.030$$

References

[1] G. Kieslich, S. Sun, and T. Cheetham. An Extended Tolerance Factor Approach for Organic-Inorganic Perovskites. *Chem. Sci.*, 6:3430–3433, 2015.

[2] C. C. Stoumpos, C. D. Malliakas, and M. G. Kanatzidis. Semiconducting tin and lead iodide perovskites with organic cations: phase transitions, high mobilities, and near-infrared photoluminescent properties. *Inorganic chemistry*, 52(15):9019–9038, aug 2013.